STRUCTURAL CONTROL AND HEALTH MONITORING
Struct. Control Health Monit. 2017;**24**:e1926.
Published online 11 August 2016 in Wiley Online Library (wileyonlinelibrary.com). DOI: 10.1002/stc.1926

High-speed 6-DOF structural displacement monitoring by fusing ViSP (Visually Servoed Paired structured light system) and IMU with extended Kalman filter

H. Jeon[1], S. Choi[2], J.-U. Shin[2], Y. Kim[2] and H. Myung[2,*,†]

[1]*Dept. Civil and Environmental Engineering, Hanbat National University, 125 Dongseo-daero, Yuseonggu, Daejeon, 34158, Korea*
[2]*Urban Robotics Lab., KAIST, 291 Daehak-ro, Yuseonggu, Daejeon, 34141, Korea*

SUMMARY

In previous studies, a visually servoed paired structured light system (ViSP) was proposed to estimate structural displacement with high accuracy at low cost. Although the performance of the system has been verified from various simulations and experimental tests, it has a limitation that high-speed dynamic displacement cannot be measured properly due to the relatively low sampling rate. To speed up ViSP, in this paper, an inertial measurement unit (IMU) with a high sampling rate is concurrently used with ViSP in a Kalman filtering framework. By combining measured accelerations and angular velocities from the IMU with the estimated 6-DOF displacement from ViSP, high-speed structural movement can be monitored with high accuracy. In the proposed data fusion method, named ViSP-IMU, random biases of the IMU are calibrated by using the estimated displacement results from ViSP-IMU. We perform experimental tests and verify the efficacy of the proposed algorithm as a promising structural displacement estimation method which guarantees high accuracy and a high sampling rate. Also, the proposed bias compensation method can effectively reduce the displacement estimation error by minimizing the difference between estimated displacements from the IMU and ViSP-IMU. Copyright © 2016 John Wiley & Sons, Ltd.

Received 11 July 2014; Revised 14 July 2016; Accepted 15 July 2016

KEY WORDS: structural health monitoring (SHM); displacement measurement; data fusion; Kalman filter; visually servoed paired structured light system (ViSP); inertial measurement unit (IMU)

1. INTRODUCTION

In the field of civil engineering, structural displacement is considered as one of important indicators to access or evaluate the structural safety. For this reason, many researchers have studied on development of displacement estimation method or system using commercial sensors such as accelerometers, Global Positioning System (GPS), Laser Doppler Vibrometers (LDVs), or a combination of different sensors [1–7]. Because of the cost effectiveness of the accelerometer, displacement estimation schemes using double integration of accelerations have been widely studied [1,6]. However, this approach has drawbacks that the estimated displacement is neither stable nor accurate because the signals from the accelerometer are sensitive to temperature changes and there is a signal drift at low frequency; the Real Time Kinematic (RTK)-GPS and LDV guarantee high accuracy; however, the costs are very high.

In recent decades, vision-based displacement measurement systems that directly measure the displacement with relatively high accuracy have been studied with the aid of hardware and software advances [8–13]. Most vision-based displacement measurement systems install artificial markers on

*Correspondence to: H. Myung, Urban Robotics Lab., KAIST, 291 Daehak-ro, Yuseonggu, Daejeon, 34141, Republic of Korea.
†E-mail: hmyung@kaist.ac.kr

the structure and a vision sensor located on a fixed position from afar captures an image of the markers. By calculating the movement of the markers, the structural behavior can be monitored. Although vision-based displacement measurement systems directly estimate structural displacement with high accuracy at low cost, they are highly sensitive to changing external environmental conditions.

To resolve these problems, a vision and laser-based paired structured light (SL) system was proposed by Myung *et al*. The system consists of two screens facing each other, each with one or two lasers and a camera [14,15]. The lasers on both sides project parallel beams to the screen on the opposite side, and the camera, which is located close to the screen, captures the image of the screen. As the distance between the screen and the camera becomes small, the system becomes more robust to environmental changes. The relative 6-DOF displacement between the two sides can be estimated by calculating the positions of the projected laser beams. Because the paired SL system can estimate the displacement only when all three laser beams are projected inside the screen boundaries, a more advanced version of the paired SL system, a visually servoed paired SL system (ViSP), has been developed [16–19]. A 2-DOF manipulator is attached to each side of the system and it controls the pose of the lasers such that the laser beams are always projected on the screen.

By calculating the positions of the projected laser beams and rotation angles of the manipulators, the 6-DOF displacement between the two sides can be estimated. Although the performance of the system and applicability to civil structures such as buildings or bridges have been validated through field tests [19], the sampling rate of the system is relatively low (e.g., less than 5 Hz) because of the latency of the communication modules.

To mitigate the drawbacks of the aforementioned sensors and systems, data fusion methods using multiple sensors have been studied for structural health monitoring (SHM). For example, the Kalman filtering method has been widely used to fuse data such as measured displacement from GPS, vision-based displacement measurement systems, and displacement reconstructed using an accelerometer [5]. In [5], a multi-rate Kalman filtering method was proposed to estimate displacements and velocities by using an accelerometer with a relatively high sampling rate in the prediction step, and by using a displacement measurement sensor with a low sampling rate in observation and update steps. Afterwards, the smoothing algorithm has been used for removing the noise. Here, it is assumed that acceleration and displacement measurements are synchronized; that is, the ratio of the sampling time intervals is an integer. Hwang *et al*. verified different types of displacement estimation methods using GPS and an accelerometer with simple integration approaches [6] and Park *et al*. proposed a displacement estimation method using an accelerometer and strain gauge measurements [7]. Most studies use accelerometers to increase the sampling rate of the measurement; however, the random biases of the accelerometers are not considered or they usually estimate 2 or 3-DOF translational displacement.

In this paper, ViSP-IMU and ViSP combined with a high-speed inertial measurement unit (IMU) is proposed to estimate the dynamic 6-DOF displacement of structures with high accuracy and a high sampling rate. To fuse data from ViSP and the IMU, an extended Kalman filter (EKF) with error models is designed. The estimated displacement and its covariance are recalculated by using a covariance intersection method. Also, the biases of the accelerometer and the gyroscope are calculated and compensated to minimize the difference in the estimated displacements from the IMU and ViSP-IMU. The rest of this paper is organized as follows. In Section 2, the structure and kinematics of ViSP are briefly introduced. A Kalman filtering scheme for fusing ViSP and IMU data with covariance intersection and bias compensation is proposed in Section 3. In Section 4, the usefulness of the proposed algorithm is validated with experiments. Finally, conclusions are drawn in Section 5.

2. VISUALLY SERVOED PAIRED STRUCTURED LIGHT SYSTEM

2.1. Structure of visually servoed paired structured light system

A concept of the structural displacement estimation using a visually servoed paired SL system (ViSP) is illustrated in Figure 1 [16]. As shown in the figure, multiple ViSPs are installed in a cascaded manner to monitor the entire structure. A schematic diagram of a single module of ViSP is shown in the box with the dotted line. As the figure shows, ViSP is composed of two sides facing each other, each with one or two lasers, a camera, and a screen. The lasers project parallel beams to the screen on the

DOI: 10.1002/stc

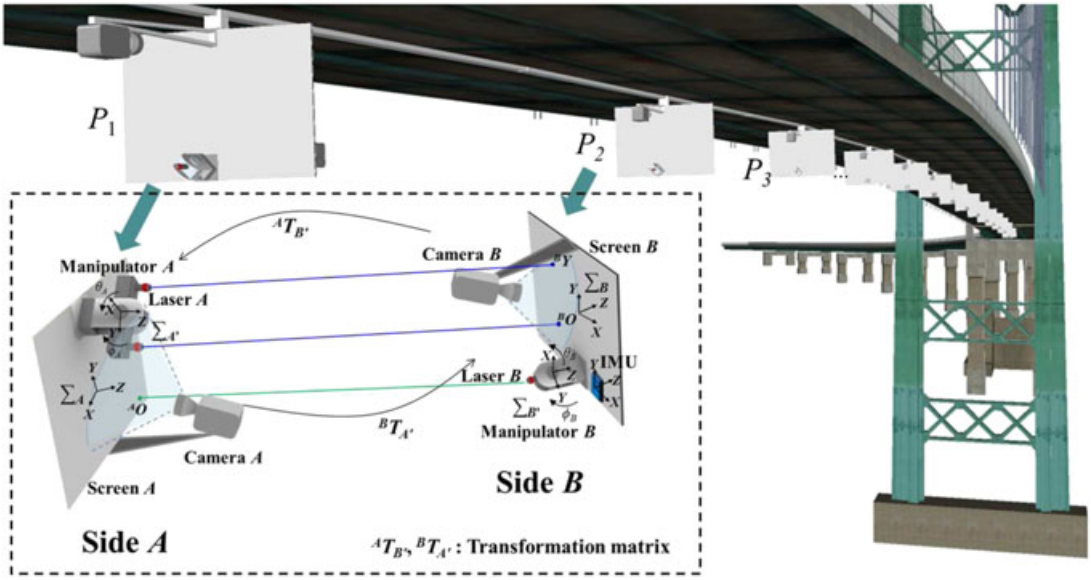

Figure 1. A schematic diagram of multiple visually servoed paired structured light systems (ViSPs) with an IMU. A composition of a single ViSP is shown in the box with the dotted line. (Modified from [18]. *Source*: Courtesy of IOP Publishing.)

opposite side and the camera near the screen captures the image of the screen. To prevent the laser beams from projecting outside the screen boundary, a 2-DOF manipulator that holds the laser(s) forces the beams to be on the screen all the time. As the distance between the screen and the camera becomes small, approximately 20 cm, the system becomes robust to environmental changes. The 6-DOF relative displacement between two sides can be estimated by calculating the positions of the projected laser beams and the rotation angles of the manipulators. For further details of ViSP, refer to [16].

2.2. Kinematics of visually servoed paired structured light system

Referring to Figure 1, the kinematics of ViSP is derived from a geometric relationship between the observed data $m = [^{A}O,\ ^{B}O,\ ^{B}Y]^{T}$ and the displacement $p = [x, y, z, \theta, \phi, \psi]^{T}$ by using homogeneous transformation matrices $^{A}T_{B}$ and $^{B}T_{A}$. Here, m indicates positions of the three projected laser beams on screen A and B; p is the 6-DOF translational and rotational displacements; and $^{A}T_{B}$ is the homogeneous transformation matrix that transforms the coordinate from screen B (Σ_B) to screen A (Σ_A), respectively.

^{A}O is the coordinate point of the projected laser beam on Screen A; ^{B}O and ^{B}Y are the coordinate points of the projected laser beams on Screen B; x, y, and z are the relative translational displacement in X, Y, and Z axes between Σ_A and Σ_B; and θ, ϕ, and ψ are the relative rotational displacement about X, Y, and Z axes between Σ_A and Σ_B. By using the transformation matrices and installed laser positions, ^{A}O can be obtained as follows:

$$^{A}O = {}^{A}T_{B}.{}^{B}T_{B'}\cdot[0\ \ 0\ \ Z_{AB}\ \ 1]^{T} \tag{1}$$

where Z_{AB} is the distance between the two sides and $^{B}T_{B'}$ is a transformation matrix from $\Sigma_{B'}$ to Σ_B which is composed of rotation angles of the manipulator on side B. In the same way, ^{B}O and ^{B}Y can be calculated by using $^{B}T_{A}$ and $^{A}T_{A'}$ as follows:

$$^{B}O = {}^{B}T_{A}.{}^{A}T_{A'}\cdot[-L_x\ \ 0\ \ Z_{AB}\ \ 1]^{T} \tag{2}$$

$$^{B}Y = {}^{B}T_{A}.{}^{A}T_{A'}\cdot[\ L_x\ \ 0\ \ Z_{AB}\ \ 1]^{T} \tag{3}$$

where L_x is the offset of the installed laser from the center of the screen in X direction. Based on the fact that z components of ^{A}O, ^{B}O, and ^{B}Y are zero because they are projected onto the 2D screen, the kinematic equation can be derived as follows:

DOI: 10.1002/stc

$$M = \left[{}^{A}O_x \; {}^{A}O_y \; {}^{B}O_x \; {}^{B}O_y \; {}^{B}Y_x \; {}^{B}Y_y \right]^T \tag{4}$$

where ${}^{A}O_x$ and ${}^{A}O_y$ denote the x and y components of ${}^{A}O$, etc.

The block diagram of the displacement estimation using ViSP is shown in Figure 2. As shown in the figure, the camera on each side captures the image of the screen and the lens distortion is corrected by using the camera's intrinsic parameters. Using the undistorted image, the screen boundary and positions of the projected laser beams are calculated based on the homography transformation. Before the projected laser beams leave the screen boundary, the 2-DOF manipulators control the pose of lasers such that the projected laser beams remain on the screen. Afterwards, the relative displacement between the two sides is calculated by using the positions of the projected laser beams and the rotation angles of the manipulators. Further details can be found in [16].

3. DATA FUSION OF VISP AND IMU: VISP-IMU

Before introducing the procedure of data fusion of ViSP and IMU, the sampling time notations should be explained. As shown in Figure 3, the sampling periods of ViSP and IMU are T_1 and T_2, respectively. Let us denote the time steps as s and k for sampling periods T_1 and T_2, respectively. Also, $s+nT_1$ and $k+jT_2$ are abbreviated as s_n and k_j, respectively. The entire procedure of the 6-DOF displacement estimation using ViSP and IMU (ViSP-IMU in short) is shown in Figure 4. As shown in the figure, data from the IMU with a higher sampling rate are used to predict the translational and rotational displacements, $\widehat{p}_I\left(k_j|k_{j-1}\right)$, until the measurement from ViSP is obtained. After receiving data from ViSP, as shown in step 2, ViSP updates the previously estimated displacement by using observed data m. In the displacement estimation using the EKF, however, errors can be induced due to the time-gap of captured images from two cameras of ViSP. Therefore, the estimated displacement and its covariance are recalculated using a covariance intersection method, as described in step 3 and further elaborated in Section 3.2. After the recalculation, the translational and rotational displacements from the IMU within T_1 are compensated based on the estimated displacement from ViSP-IMU.

3.1. Extended Kalman filtering method

In the fusion of ViSP and IMU with different sampling rates, the EKF can be applied to estimate the displacement. The EKF is composed of three steps; prediction, observation, and update steps. In the

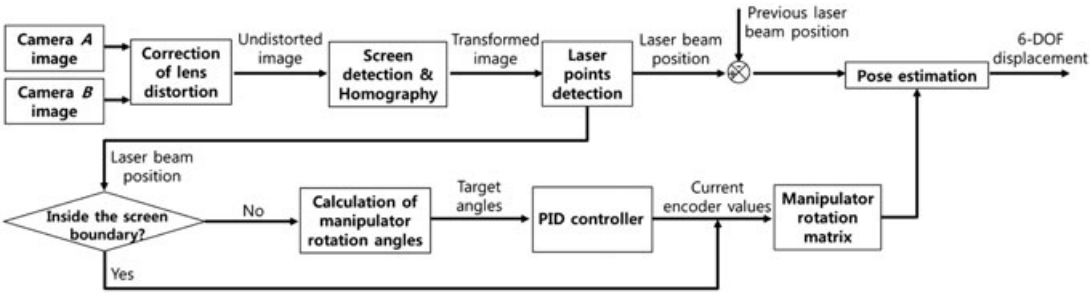

Figure 2. A block diagram of the displacement estimation using a visually servoed paired structured light system (ViSP). (Modified from [16]. *Source*: Courtesy of IOP Publishing.)

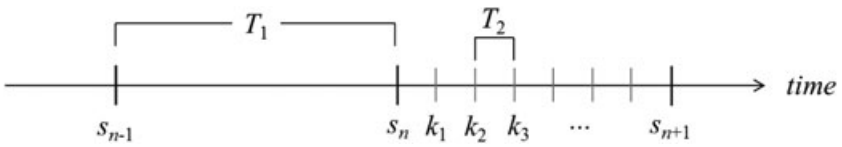

Figure 3. The sampling times of the measurement data from ViSP and IMU are T_1 and T_2, respectively.

DOI: 10.1002/stc

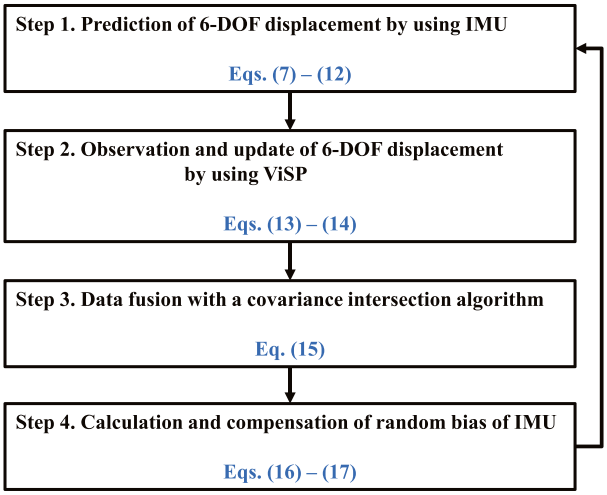

Figure 4. Procedure of 6-DOF displacement estimation for ViSP-IMU.

prediction step of the EKF, the 6-DOF translational and rotational displacements can be estimated by using a tri-axial accelerometer and gyroscope, respectively. In this paper, the translational displacement is obtained by minimizing the difference between estimated and measured accelerations as follows:

$$\arg\min_{\widehat{p}_{I(t)}} \frac{1}{2} \sum_{i=j-N_f}^{j} \left(\widehat{a}_{k_i}\left(\widehat{p}_{I(t)}\right) - \overline{a}_{k_i}\right)^T \left(\widehat{a}_{k_i}\left(\widehat{p}_{I(t)}\right) - \overline{a}_{k_i}\right) \tag{5}$$

where $\widehat{a}_{k_i}$ and $\overline{a}_{k_i}$ are the estimated and the measured accelerations at time k_i, respectively. $\widehat{p}_{I(t)}$ denotes the estimated translational displacement by using data from an IMU and N_f is the number of data within a finite time interval which is normally decided based on the first natural frequency of the target structure. In [1], N_f is set to $N_r f_s / f_1 + 1$ where N_r, f_s, and f_1 are the ratio of the time-window size, the sampling rate, and the first natural frequency, respectively. Note that $\widehat{a}_{k_i}$ is a function of $\widehat{p}_{I(t)}$ and can be calculated by using a finite difference method [1,20] represented as

$$\widehat{a}_{k_i} = \frac{\widehat{p}_{I(t)}(k_{i+1}) - 2\widehat{p}_{I(t)}(k_i) + \widehat{p}_{I(t)}(k_{i-1})}{{T_2}^2} \tag{6}$$

where $i = j, j-1, \cdots, j-N_f$. Substituting Eq. (6) into Eq. (5), $\widehat{p}_{I(t)}$ can be obtained as follows [1]:

$$\widehat{p}_{I(t)}(k_j) = \left(\mathbf{L}_{(t)}^T \mathbf{L}_{(t)}\right)^{\dagger} \mathbf{L}_{(t)}^T \mathbf{L}_i \overline{\mathbf{a}} {T_2}^2 \tag{7}$$

where the subscript (t) denotes the translational component of the displacement, $\bar{\mathbf{a}}$ is the measured acceleration vector, and $\left(\mathbf{L}_{(t)}^T \mathbf{L}_{(t)}\right)^{\dagger}$ is the pseudo-inverse of the $\mathbf{L}_{(t)}^T \mathbf{L}_{(t)}$. $\mathbf{L}_{(t)} = \mathbf{L}_i \mathbf{L}_h$, where $\mathbf{L}_i$ is an integration operator of the finite difference method with an odd number of time steps, and $\mathbf{L}_h$ is a second-order derivative operator as follows:

$$\mathbf{L}_{\mathrm{i}} = \begin{bmatrix} \frac{1}{\sqrt{2}} & & & & \\ & 1 & & 0 & \\ & & \ddots & & \\ & 0 & & 1 & \\ & & & & \frac{1}{\sqrt{2}} \end{bmatrix} \tag{8}$$

DOI: 10.1002/stc

$$\mathbf{L}_{\mathrm{h}} = \begin{bmatrix} 1 & -2 & 1 & & & & \\ & 1 & -2 & 1 & & 0 & \\ & & & \ddots & & & \\ & 0 & & 1 & -2 & 1 & \\ & & & & 1 & -2 & 1 \end{bmatrix} \tag{9}$$

Similar to Eq. (7), the rotational displacement using the measured angular velocities can be estimated as follows:

$$\widehat{p}_{I(r)}(k_j) = \left(T_2{}^2\mathbf{L}_{(r)}^T\mathbf{L}_{(r)}\right)^{\dagger}\mathbf{L}_{(r)}^T\mathbf{L}_i\overline{\mathbf{v}}T_2{}^3 \tag{10}$$

where the subscript (r) denotes the rotational component of the displacement and $\overline{\mathbf{v}}$ is the measured angular velocity vector. $\mathbf{L}_{(r)} = \mathbf{L}_i\mathbf{L}_g$, where $\mathbf{L}_g$ is a first-order derivative operator defined as follows:

$$\mathbf{L}_{\mathrm{g}} = \begin{bmatrix} 1 & -1 & & & & \\ & 1 & -1 & & 0 & \\ & & & \ddots & & \\ & 0 & & 1 & -1 & \\ & & & & 1 & -1 \end{bmatrix} \tag{11}$$

By combining the equations, *a priori* displacement can be obtained as follows:

$$\widehat{p}_I(k_j|k_{j-1}) = \begin{bmatrix} \widehat{p}_{I(t)}(k_{j-1}) + \Delta\widehat{p}_{I(t)}(k_j|k_{j-1})\Delta k_j/T_2 \\ \widehat{p}_{I(r)}(k_{j-1}) + \Delta\widehat{p}_{I(r)}(k_j|k_{j-1})\Delta k_j/T_2 \end{bmatrix} \tag{12}$$

where $\widehat{p}_I = \left[\widehat{p}_{I(t)};\ \widehat{p}_{I(r)}\right]$, $\Delta\widehat{p}_I(k_j|k_{j-1}) = \widehat{p}_I(k_j) - \widehat{p}_I(k_{j-1})$, and $\Delta\mathrm{k}_j$ is the time gap between the currently obtained IMU data and the previously obtained IMU or ViSP data. The prediction step is performed whenever tri-axial accelerations and angular velocities are obtained until the data from ViSP are observed; that is, Eqs. (7)–(12) are performed with $j = 1, \ldots, N_{\mathrm{IMU}}$, where N_{IMU} is the number of measured accelerations and angular velocities within T_1. Instead of using EKF, the Runge–Kutta method could have been used when the computational cost is low, and the velocity and acceleration information is obtainable by differentiation of the displacement.

After receiving data from ViSP, the following observation and update steps are performed. In the observation step of the EKF, the following equation is applied:

$$\begin{aligned} \widehat{p}_I(s_n|k_N) &= \widehat{p}_I(k_N|k_{N-1}) + (\widehat{p}_I(k_N|k_{N-1}) - \widehat{p}_I(k_{N-2}|k_{N-1}))\Delta s_n/T_2 \\ m(s_n|k_N) &= M(\widehat{p}_I(s_n|k_N)) \\ v(s_n) &= m(s_n) - \widehat{m}(s_n|k_N) \\ P_V(s_n|s_{n-1}) &= P_V(s_{n-1}|s_{n-1}) + Q \\ S(s_n) &= JP_V(s_n|s_{n-1})J^T + R \end{aligned} \tag{13}$$

where k_N is an abbreviation for $k_{N_{\mathrm{IMU}}}$, $J = \partial M/\partial\widehat{p}_I(s_n|k_N)$ is the Jacobian of the kinematic equation M, Q is the covariance matrix of system noise of ViSP, R is the covariance matrix of the measurement noise of ViSP, and P_V is the error covariance matrix of the displacement from ViSP.

DOI: 10.1002/stc

The update step can be obtained as follows:

$$\begin{aligned} K(s_n) &= P_V(s_n|s_{n-1})J^T S(s_n) \\ \widehat{p}_V(s_n|s_n) &= \widehat{p}_I(s_n|k_N) + K(s_n)v(s_n) \\ P_V(s_n|s_n) &= P_V(s_n|s_{n-1}) - K(s_n)S(s_n)K^T(s_n). \end{aligned} \tag{14}$$

Because the data from the IMU and ViSP are obtained at different sampling rates and the IMU is faster than ViSP, the prediction step is performed with the sampling rate of the IMU, and the observation and update steps are performed with the sampling rate of ViSP.

3.2. Covariance intersection method

Before starting the displacement estimation, the wireless communication latency between two sides is measured multiple times and the instances of grabbing images from the cameras are synchronized by considering the average of the measured latencies. Although the synchronization algorithm is performed at the beginning, there can be a time gap of grabbing images due to the variance of the measured latency and an inconsistent time delay of grabbing images. The time gap between the two sides results in discrepancy in displacement estimation between ViSP and the IMU, especially in the case of movement with high frequency. To reduce the discrepancy, a simple covariance intersection method that quickly combines estimated displacements considering their covariances and frequency components has been employed. This covariance intersection method will reduce the difference in displacement estimation between ViSP and the IMU. As described in Eq. (15), the method combines variables in the Kalman filter without knowing the correlation between them [21].

$$\begin{aligned} P_{F-1}(s_n|k_N) &= wP_I^{-1}(s_n|k_N) + (1-w)P_V^{-1}(s_n|s_n), \\ \widehat{p}_F(s_n|k_N) &= P_F(s_n|k_N)\left(wP_I^{-1}(s_n|k_N)\widehat{p}_I(s_n|k_N) + (1-w)P_V^{-1}(s_n|s_n)\widehat{p}_V(s_n|s_n)\right) \end{aligned} \tag{15}$$

where w[†] is the weight factor, $\widehat{p}_F(s_n|k_N)$ is the estimated displacement from ViSP-IMU at time s_n, and $P_F(s_n|k_N)$ is the error covariance of $\widehat{p}_F(s_n|k_N)$. $\widehat{p}_I(s_n|k_N)$ and $\widehat{p}_V(s_n|s_n)$ are the estimated displacements, and $P_I(s_n|k_N)$ and $P_v(s_n|s_n)$ are their error covariances at time s_n for the IMU and ViSP, respectively. The initial values of $P_F(s_n|k_N)$ and $P_V(s_n|s_n)$ can be calculated from some experimental tests. As stated in more detail in Section 4, ViSP and an IMU are installed on a motorized motion-stage which can generate a precise repeated movements. And the error covariance matrices of ViSP and the IMU can be calculated based on the difference between the ground truth obtained from the motion-stage and the measured value from ViSP and the IMU. After obtaining initial error covariances, $P_I(s_n|k_N)$ is not updated because $\widehat{p}_I(s_n|k_N)$ does not have any update equation unlike $\widehat{p}_V(s_n|s_n)$.

The weight factor, w, is determined based on the calculated normalized frequency, the dominant frequency over the predefined first natural frequency, within a finite time interval. The normalized frequency can be calculated by dividing the signal's first natural frequency by the sampling frequency. This weight factor is usually set heuristically. For example, if the normalized frequency is greater than 1.0, the w is set to a value greater than 0.5; otherwise it is set to a value less than 0.5. In other words, the predicted displacement from the IMU is dominantly used to estimate high frequency displacement. Otherwise, the estimated displacement from ViSP-IMU is dominantly used.

3.3. Compensation of random bias of inertial measurement unit

Because the accelerometers and gyroscopes have bias instabilities [22,23], they should be compensated to increase the accuracy of the estimated displacement from the IMU. In this paper, the bias of the IMU is estimated by minimizing the difference between the estimated displacements from the IMU and ViSP-IMU. By using the estimated displacement from the EKF with the covariance intersection

[†]Correction added on 18 August 2016, after first online publication: "w" was omitted from the first line after Eq. 15; this has now been corrected.

DOI: 10.1002/stc

method, the bias of the IMU within the previous T_1 is calculated as follows:

$$\begin{aligned} E(s_n) &= \widehat{p}_F(s_n|k_N) - \widehat{p}_I(s_n|k_N) \\ \Sigma_k &= \textstyle\sum_{j=1}^{N_{\mathrm{IMU}}} \Delta k_j \\ \Sigma_{k^2} &= \textstyle\sum_{j=1}^{N_{\mathrm{IMU}}} \Delta k_j^2 \\ B_a &= 2E_{(t)}(s_n)/\Sigma_{k^2} \\ B_g &= E_{(r)}(s_n)/\Sigma_k \end{aligned} \tag{16}$$

where $\Delta k_j = k_j - k_{j-1}$, where k_j is the time stamp of the j-th IMU data within T_1 and k_0 is the time stamp of the previous ViSP data; and B_a and B_g are calculated random biases of the tri-axial accelerometer and gyroscope, respectively.

In Eq. (16), the biases are calculated based on the assumption that the biases within T_1 are identical and the computed error $E(s_n)$ is equally divided based on the time interval Δk_j. After calculating the random biases, the estimated displacements between s_{n-1} and s_n are updated as follows:

$$\begin{aligned} \widehat{p}_{F(t)}\left(k_j|k_{j-1}\right) &= \widehat{p}_{I(t)}\left(k_j|k_{j-1}\right) + 0.5B_a\Delta k_j^2 \\ \widehat{p}_{F(r)}\left(k_j|k_{j-1}\right) &= \widehat{p}_{I(r)}\left(k_j|k_{j-1}\right) + B_g\Delta k_j \end{aligned} \tag{17}$$

where $j = 1, \ldots, N_{\mathrm{IMU}}$.

4. EXPERIMENTAL TESTS

To evaluate the performance of the proposed method, experimental tests using a shaking table or a motorized motion-stage have been performed. The sampling frequencies of the IMU (MTi-30, Xsens Inc. [24]) and ViSP are set to 100 Hz and 5 Hz, respectively. The covariance matrices were carefully tuned through various tests, as shown in Table I. Specifically, the ViSP and an IMU are installed on the motion-stage which can generate a precise repeated movements, for example, ± 10.0 mm in X-axis or ± 1.0 deg around Y-axis. The covariance matrices of ViSP and the IMU can be calculated based on the difference between the ground truth obtained from the motion-stage and the actual measured values from ViSP and the IMU.

The experimental setup is shown in Figure 5. For translation experiments, as shown in Figure 5(a), one of the two sides of ViSP is laid on a two-story steel frame model building excited by a shaking table, and the other is situated on a fixed table at a distance of 1.5 m. The IMU sensor is installed at side B of ViSP to test the proposed method with high-speed, as shown in Figure 5(b). The shaking table is used to create artificial movements between the two sides, and a one-dimensional laser distance sensor (CD4-350, OPTEX FA Co., Ltd. [25]) is used for comparison with the estimated displacement from the proposed system. For the rotation experiment, a very accurate motion-stage has been used to create artificial movements as shown in Figure 5(c). The motion-stage offers a resolution of 29 nm and 5 arcmin for translational and rotational movements, respectively [26].

Table I. Covariances of ViSP and IMU (unit: cm^2 or deg^2).

Type of sensor	Covariance		Value
ViSP	P_V	$P_{V(t)}(0)$	$1\times10^{-1}I_{3\times3}$
		$P_{V(r)}(0)$	$3\times10^{-1}I_{3\times3}$
	Q	$Q_{(t)}$	$5\times10^{-2}I_{3\times3}$
		$Q_{(r)}$	$1\times10^{-5}I_{3\times3}$
	R		$5\times10^{-2}I_{6\times6}$
IMU	P_I	$P_{I(t)}$	$5\times10^{-2}I_{3\times3}$
		$P_{I(r)}$	$1\times10^{-5}I_{3\times3}$

ViSP, visually servoed paired structured light system; IMU, inertial measurement unit.

DOI: 10.1002/stc

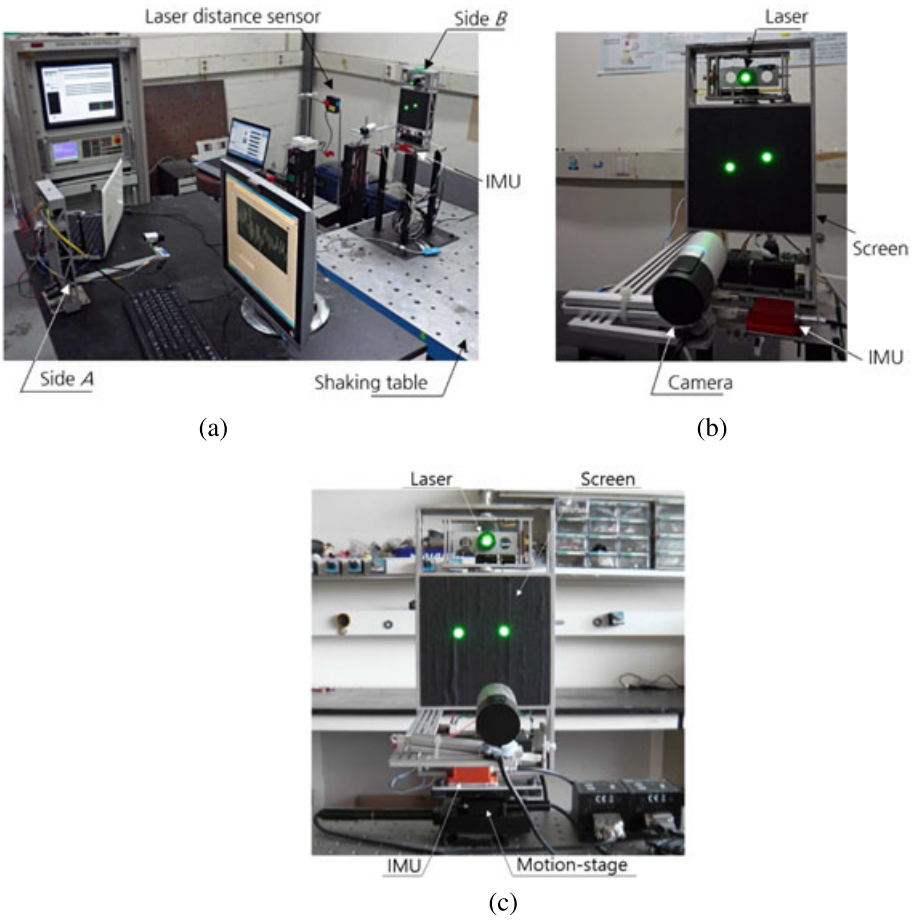

Figure 5. The experimental setup. (a) One of two sides of ViSP, side *A*, is installed on the fixed table and the other, side *B*, on the shaking table with an IMU. (b) The details of side *B* of ViSP. (c) ViSP on a motion-stage for rotation experiments.

In this paper, two types of input voltage were applied to the shaking table for the translation experiments: a sinusoidal sweep signal from 1 to 4 Hz and a random signal within 10 Hz. The sampling frequencies are chosen based on the consideration that the most civil structures have a major frequency less than 10 Hz [27]. For the rotation experiment, the motion-stage created movements with 0.28 Hz sinusoidal input.

In the displacement prediction step using the IMU, the finite time interval is set based on the first natural frequency of three cases, such as 1 Hz; w in the covariance intersection method is determined based on the normalized frequency. In the experiments, if the normalized frequency is greater than 1.0, the w is set to 0.8; otherwise it is set to 0.2.

It should be noted that a low pass filter with a cut off frequency at 20 Hz has been used to reduce the signal drift and noise of the sensor, especially the accelerometer. The cut off frequency has been chosen based on the consideration that most civil structures have a major frequency less than 10 Hz and the Nyquist theorem.

Figure 6(a) shows the estimated displacement by ViSP-IMU and the laser distance sensor with a sinusoidal sweep input. Figure 6(b) shows a magnified plot of Figure 6(a) including the estimated displacements from ViSP, IMU, and ViSP-IMU with and without bias compensation between 25.6 and 26.6 sec. To verify the performance of the proposed bias compensation method, a well-known Rauch-Tung-Striebel (RTS) smoother with the EKF was compared. Figure 7(a) shows the estimated displacement with a random input. Figure 7(b) shows a magnified plot of Figure 7(a) including the estimated displacements from ViSP, IMU, and ViSP-IMU with and without bias compensation, and with RTS between 20.2 and 21.1 sec. Figure 8(a) shows the estimated displacement with a rotation input. Figure 8(b) shows a magnified plot of Figure 8(a) including the estimated displacements from ViSP, IMU, and ViSP-IMU with and without bias compensation, and with RTS between 26.0

DOI: 10.1002/stc

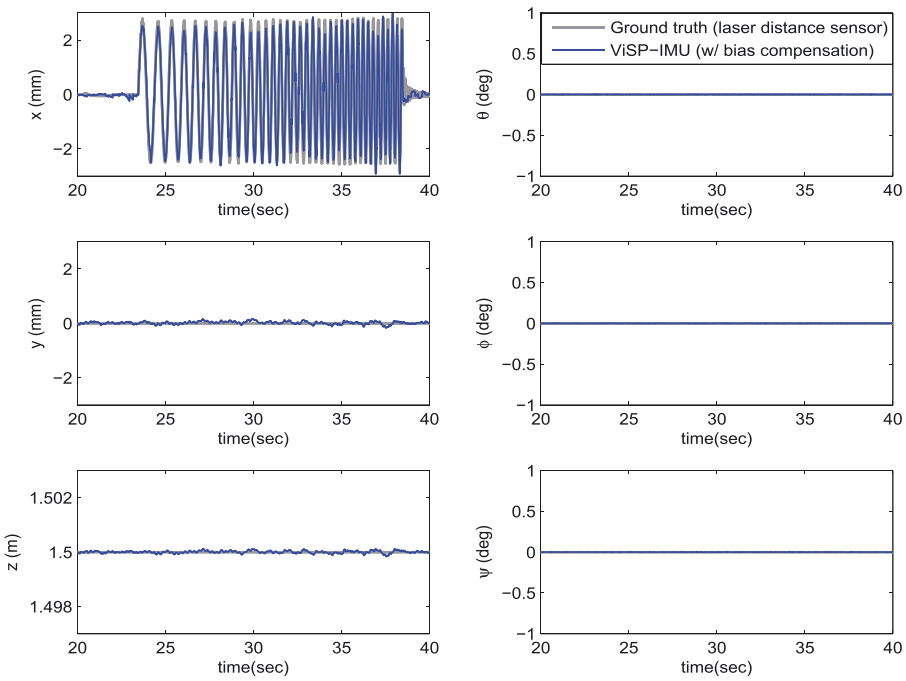

(a)

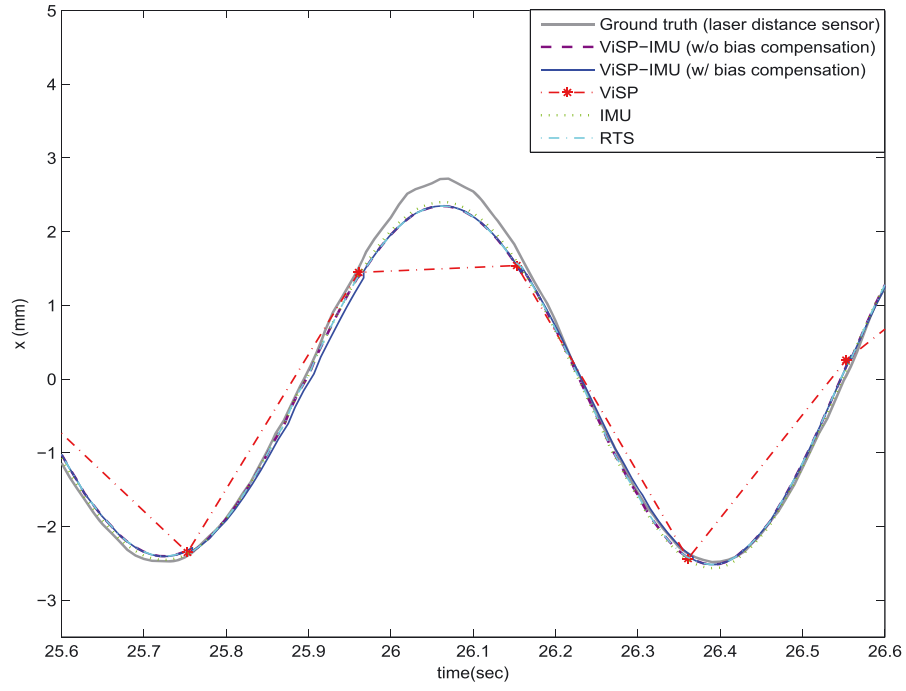

(b)

Figure 6. Experimental result for a sinusoidal sweep input. (a) Estimated 6-DOF displacement using ViSP-IMU (thin solid line) and the ground truth (gray solid line). (b) Zoomed plot of the estimated *X*-axis translational displacement using ViSP-IMU with and without the bias compensation method (thin solid line and dashed line, respectively), the ground truth (gray solid line), ViSP (dash-dotted line with asterisk), IMU (dotted line), and RTS (dash-dotted line) for 25.6 s $\leq t \leq$ 26.6 s.

and 32.0 sec. A rotational displacement experiment was carried out with ±1 degree of rotation around *Y*-axis at 2 m of distance. The effectiveness of the bias compensation method can be clearly seen in Figures 6(b), 7(b), and 8(b).

DOI: 10.1002/stc

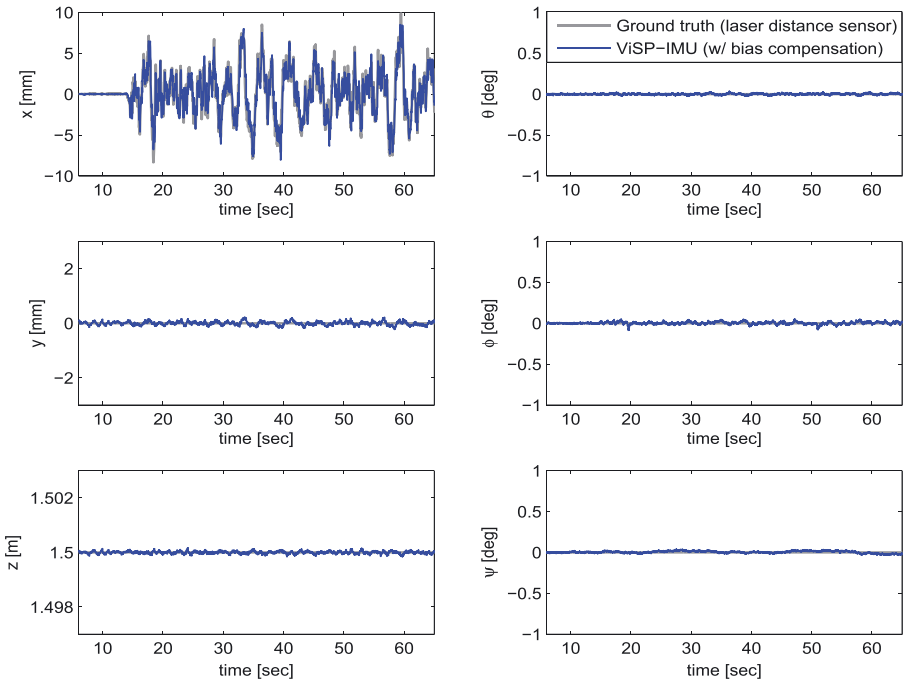

(a)

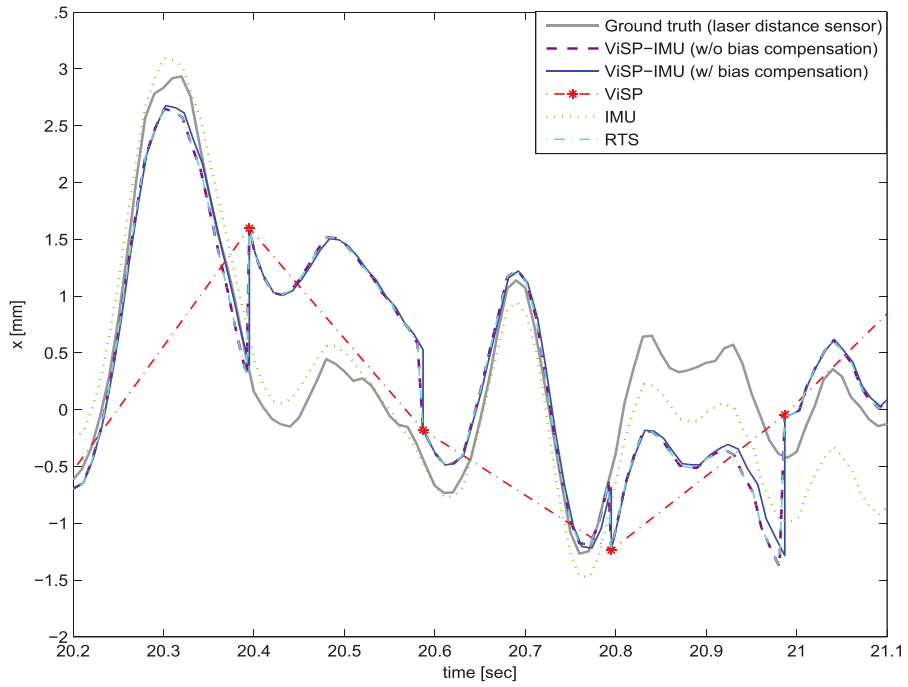

(b)

Figure 7. Experimental result for a random input. (a) Estimated 6-DOF displacement using ViSP-IMU (thin solid line) and the ground truth (gray solid line). (b) Zoomed plot of the estimated X-axis translational displacement using ViSP-IMU with and without the bias compensation method (thin solid line and dashed line, respectively), the ground truth (gray solid line), ViSP (dash-dotted line with asterisk), IMU (dotted line), and RTS (dash-dotted line) for 20.2 s $\leq t \leq$ 21.1 s.

As seen in the experimental results, the estimated displacements with the proposed method correspond to the ground truth with a high level in all cases. Also, the displacement estimation error is further reduced by using the bias compensation method.

DOI: 10.1002/stc

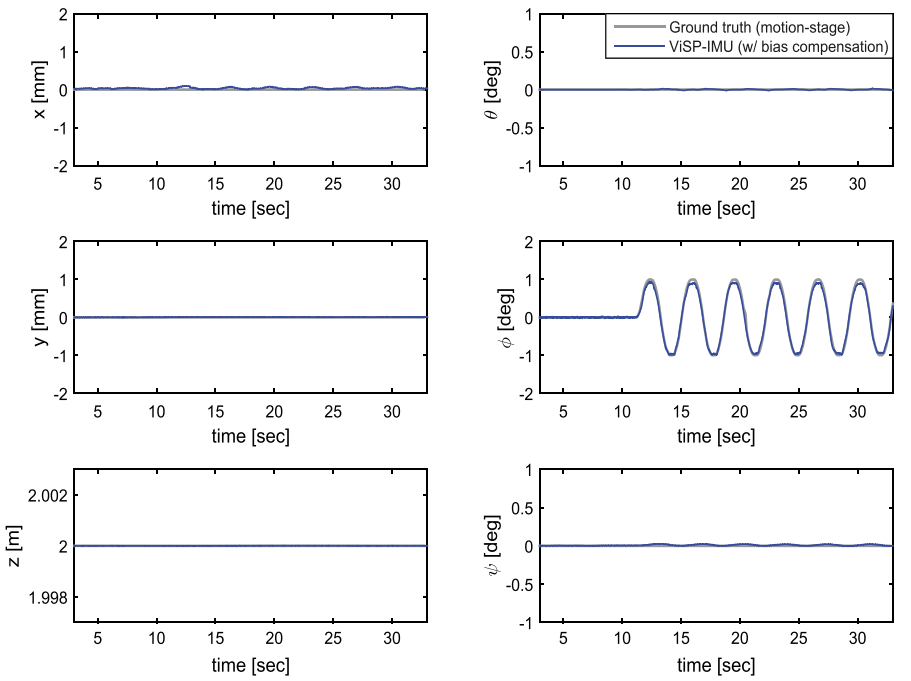

(a)

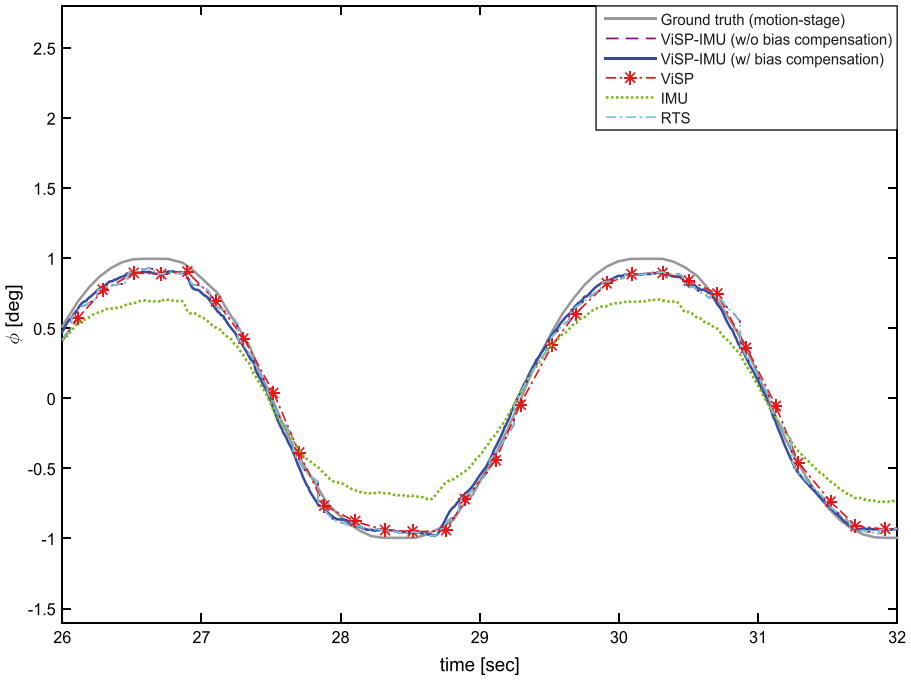

(b)

Figure 8. Experimental result for a rotating input. (a) Estimated 6-DOF displacement using ViSP-IMU (thin solid line) and the ground truth (gray solid line). (b) Zoomed plot of the estimated *Y*-axis rotational displacement using ViSP-IMU with and without the bias compensation method (thin solid line and dashed line, respectively), the ground truth (gray solid line), ViSP (dash-dotted line with asterisk), IMU (dotted line), and RTS (dash-dotted line) for 26.0 s $\leq t \leq$ 32.0 s.

The estimated results are evaluated against the ground truth based on the mean absolute errors (MAE_T and MAE_R), which are defined by the following equations:

DOI: 10.1002/stc

Table II. Mean absolute errors (MAE_T and MAE_R) for experimental tests with a sinusoidal sweep (Case 1), a random input (Case 2), and a rotation input (Case 3), respectively. The estimated displacement from ViSP-IMU with the bias compensation method shows the best performance for all cases.

Case	Algorithm	MAE_T (mm)	MAE_R(°)
Case 1	ViSP only	0.094	0.014
	IMU only	0.124	0.004
	ViSP-IMU (w/o bias comp.)	0.079	0.004
	ViSP-IMU (w bias comp.)	0.078	0.004
	RTS	0.083	0.004
Case 2	ViSP only	0.284	0.016
	IMU only	0.642	0.036
	ViSP-IMU (w/o bias comp.)	0.260	0.013
	ViSP-IMU (w bias comp.)	0.254	0.012
	RTS	0.266	0.013
Case 3	ViSP only	0.018	0.029
	IMU only	0.110	0.154
	ViSP-IMU (w/o bias comp.)	0.017	0.030
	ViSP-IMU (w bias comp.)	0.017	0.025
	RTS	0.017	0.025

ViSP, visually servoed paired structured light system; IMU, inertial measurement unit; RTS, Rauch-Tung-Striebel.

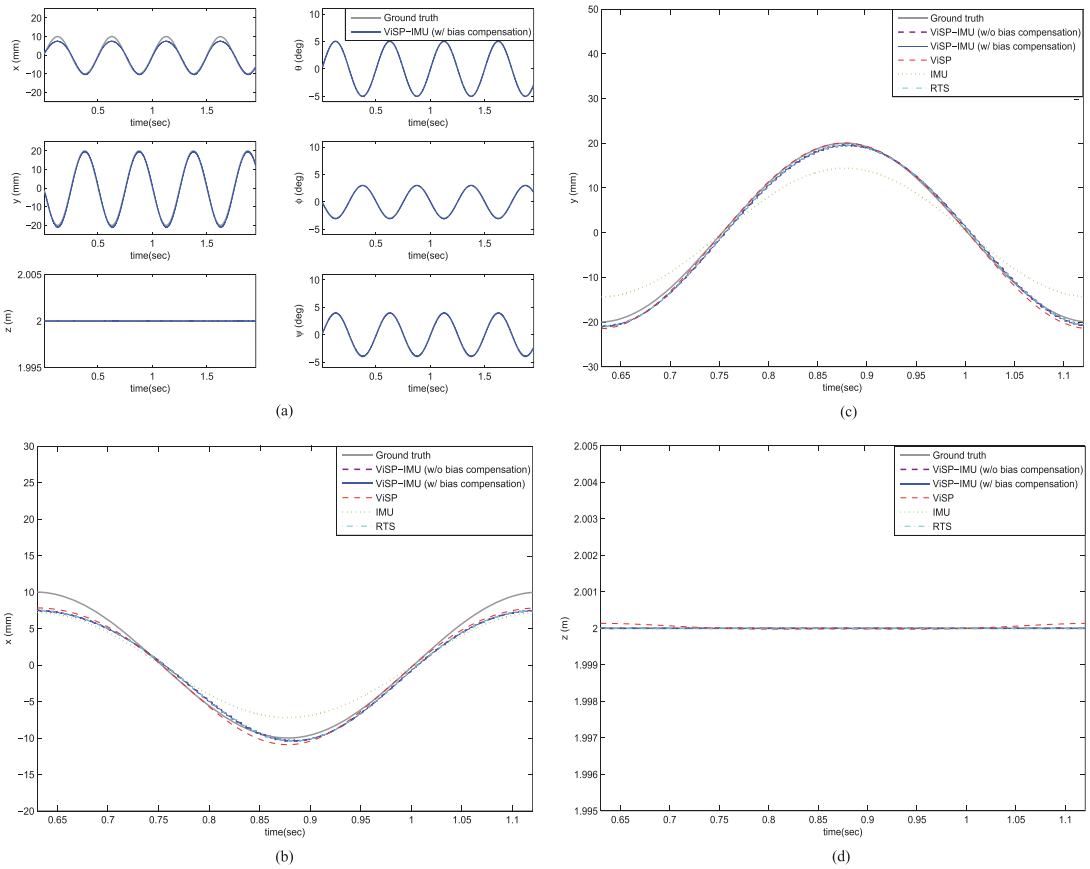

Figure 9. Simulation result for 5 axes motion. (a) Estimated 6-DOF displacement using ViSP-IMU (thin solid line) and the ground truth (gray solid line). (b) Zoomed plot of the estimated *X*-axis translational displacement using ViSP-IMU with and without the bias compensation method (thin solid line and dashed line, respectively), the ground truth (gray solid line), ViSP (thin dashed line), IMU (dotted line), and RTS (dash-dotted line) for 0.63 s $< t <$ 1.12 s. (c) Zoomed plot of the estimated translational displacement in *Y*-axis. (d) Zoomed plot of the estimated translational displacement in *Z*-axis. (e) Zoomed plot of the estimated rotational displacement about *X*-axis. (f) Zoomed plot of the estimated rotational displacement about *Y*-axis. (g) Zoomed plot of the estimated rotational displacement about *Z*-axis

DOI: 10.1002/stc

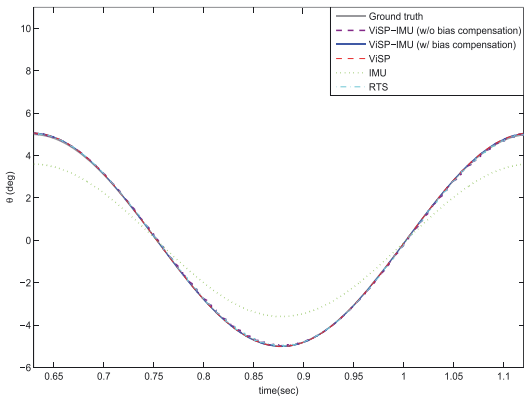

(e)

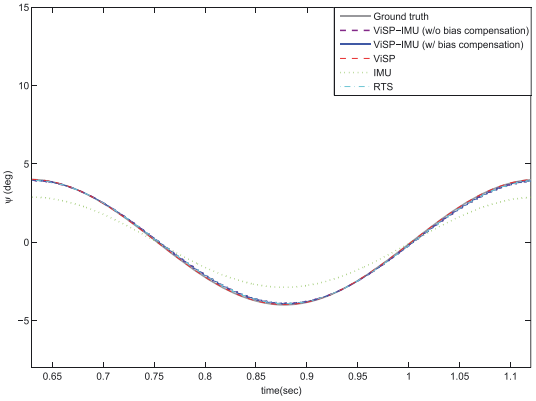

(g)

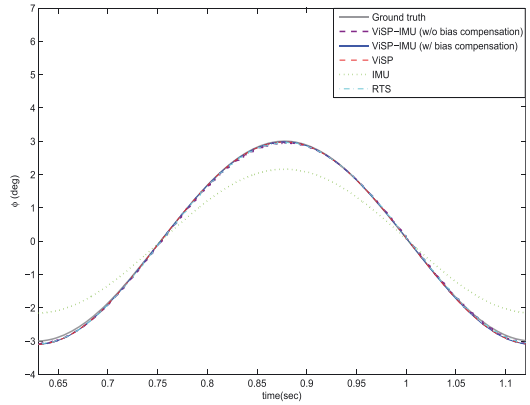

(f)

Figure 9. (Continued)

$$\mathrm{MAE}_T = \frac{\sum_{i=1}^{n}\sum_{j=1}^{3}|\widehat{p}^{j}_{i(t)} - p^{j}_{i(t)}|}{3n} \tag{18}$$

$$\mathrm{MAE}_R = \frac{\sum_{i=1}^{n}\sum_{j=4}^{6}|\widehat{p}^{j}_{i(r)} - p^{j}_{i(r)}|}{3n} \tag{19}$$

where n is the total number of data, $\widehat{p}$ is the estimated displacement by using the proposed method, p is the ground truth obtained from the laser distance sensor or the motion-stage, the subscript i indicates the i-th estimated displacement, and the superscript j indicates the j-th component of the displacement. The MAEs of the experimental tests are shown in Table II. As shown in the table, the displacement estimated using ViSP-IMU with the bias compensation method shows the smallest error.

The simulations have been conducted with respect to five axes motion generated by 2 Hz sinusoidal waves when the two sides of ViSP are located at the distance of 2 m away in Z-axis direction. Based on the artificial movement, the measurement data, which are the positions of the laser beams and the rotation angles of the manipulators, have been calculated. After the calculation, the displacements have been estimated by different methods as shown in Figure 9(b)–(g). The raw data of an IMU are acquired by the following methods. At first, a cubic interpolation is applied to the ground truth data in order to obtain 100 Hz IMU data similar to the real experimental data obtained by the Xsens IMU. Secondly, the data sampled at 100 Hz are used for calculating the acceleration by utilizing the second derivative method, called centered finite-divided-difference [28]. In the simulation, the uniform measurement noise of ±5 pixels, corresponding to ±0.93 mm and ±1.67 mm in X and Y axes, respectively, has been added to the projected laser beam positions on each screen in accordance with the characteristics of ViSP.

DOI: 10.1002/stc

Table III. Mean absolute errors (MAE_T and MAE_R) for the simulation test with a sinusoidal input. The estimated displacement from ViSP-IMU with the bias compensation method shows the best performance.

Case	Algorithm	MAE_T (mm)	MAE_R(°)
Simulation	ViSP only	0.883	0.050
	IMU only	1.813	0.725
	ViSP-IMU (w/o bias comp.)	0.534	0.050
	ViSP-IMU (w bias comp.)	0.533	0.042
	RTS	0.533	0.050

ViSP, visually servoed paired structured light system; IMU, inertial measurement unit; RTS, Rauch-Tung-Striebel.

Table IV. The components of ViSP-IMU and their prices as of July 2015.

Component	Unit Price (USD)	Quantity	Price (USD)
PC (EPICA-P830-12 L + DDR3 SO-DIMM 4GB + SSD 32GB SLC Type)	435	2 EA	870
Cameras (Logitech C2000, USA)	20	2 EA	40
Lasers (Lanics LM-6505MR, Korea)	150	3 EA	450
Bluetooth (Frimtech FB200AS, Korea)	80	2 EA	160
Motors (Maxon, USA)	220	4 EA	880
Aluminum Chassis	30(per 1 kg)	1.2 kg	36
Inertial measurement unit (Xsens MTi-30, Netherlands)	3,451	1 EA	3,451
Total		1 EA	5,887

Gaussian noise with standard deviation of 9×10^{-4} (m/s^2) and 12×10^{-4} (rad/s) for acceleration and angular velocity, respectively, has been added to the IMU data, considering the sensor characteristics of the IMU. The simulation result is shown in Figure 9 and Table III. Similar with the experimental results, the estimated displacement from ViSP-IMU with the bias compensation method shows the best performance.

5. CONCLUSIONS

This paper proposes a Kalman filter-based data fusion method to speed up a ViSP with the aid of an IMU. The 6-DOF displacement is updated by a tri-axial accelerometer and a gyroscope until the positions of the projected laser beams are obtained from ViSP. After receiving the observation data from ViSP, the displacement is updated by using an extended Kalman filter. Considering the error of ViSP at high-frequency, the covariance intersection method is applied to recalculate the 6-DOF displacement. The difference between the estimated displacements from the IMU and ViSP-IMU is considered as the error due to biases of the IMU. By minimizing the error, biases of the accelerometer and gyroscope are calculated and the previously updated displacement from the IMU is compensated. For performance evaluation of the proposed algorithm, experimental tests have been conducted.

The experimental results show that the 6-DOF displacement can be estimated with high accuracy and a high sampling rate by fusing ViSP with an IMU. Also, the bias compensation method increased the accuracy of the estimated displacement by minimizing the gap between displacements estimated from the IMU and ViSP-IMU.

The average price of the RTK GPS receiver with an accuracy of a few centimeters and a maximum sampling rate of 1–2 Hz is more than 20,000 USD. The cost of a RTK-GPS receiver for dynamic displacement measurement with a maximum sampling rate of 20–50 Hz is even higher than the static one (about 150,000 USD [3]). However, the cost of ViSP with an IMU is less than 6,000 USD (please see Table IV), which is roughly four times cheaper than the static RTK-GPS receiver and 25 times cheaper than the dynamic RTK-GPS receiver. Moreover, ViSP can provide 6-DOF displacement while the receivers usually provide 3-DOF displacement. The price can be further reduced by optimizing the software and replacing the PC with low-cost embedded processors.

DOI: 10.1002/stc

ACKNOWLEDGEMENT

This study was supported by a grant (13SCIPA01) from Smart Civil Infrastructure Research Program funded by Ministry of Land, Infrastructure and Transport (MOLIT) of Korea government and Korea Agency for Infrastructure Technology Advancement (KAIA). The students are supported by MOLIT under the U-City Master and Doctor Course Grant Program. The authors would like to thank Prof. Junhee Kim, Dankook University, for his valuable comments.

REFERENCES

1. Lee HS, Hong YH, Park HW. Design of an FIR filter for the displacement reconstruction using measured acceleration in low-frequency dominant structures. *International Journal for Numerical Methods in Engineering* 2010; **82**(4):403–434.
2. Park KT, Kim SH, Park HS, Lee KW. The determination of bridge displacement using measured acceleration. *Engineering Structures* 2005; **27**(3):371–378.
3. Casciati F, Fuggini C. Monitoring a steel building using GPS sensors. *Smart Structures and Systems* 2011; **7**(5):349–363.
4. Nassif HH, Gindy M, Davis J. Comparison of laser Doppler vibrometer with contact sensors for monitoring bridge deflection and vibration. *NDT & E International* 2005; **38**(3):213–218.
5. Smyth A, Wu M. Multi-rate Kalman filtering for the data fusion of displacement and acceleration response measurements in dynamic system monitoring. *Mechanical Systems and Signal Processing* 2007; **21**(2):706–723.
6. Hwang J, Yun H, Park SK, Lee D, Hong S. Optimal methods of RTK-GPS/accelerometer integration to monitor the displacement of structures. *Sensors* 2012; **12**(1):1014–1034.
7. Park JW, Sim SH, Jung HJ. Displacement estimation using multimetric data fusion. *IEEE/ASME Transactions on Mechatronics* 2013; **18**(6):1675–1682.
8. Chang CC, Xiao XH. Accurate displacement measurement from fusion of vision-based displacement and acceleration with Kalman filter. *Proceedings of 20th International Conference on Adaptive Structures and Technologies*, Hong Kong; 2009.
9. Stephen GA, Brownjohn JMW, Taylor CA. Visual monitoring of the Humber bridge. *Engineering Structures* 1993; **15**(3):197–208.
10. Wahbeh AM, Caffrey JP, Masri SF. A vision-based approach for the direct measurement of displacements in vibrating systems. *Smart Materials and Structures* 2003; **12**(5):785–794.
11. Lee JJ, Shinozuka M. Real-time displacement measurement of a flexible bridge using digital image processing techniques. *Experimental Mechanics* 2006; **46**(1):105–114.
12. Park JW, Lee JJ, Jung HJ, Myung H. Vision-based displacement measurement method for high-rise building structures using partitioning approach. *NDT & E International* 2010; **43**(7):642–647.
13. Ni YQ, Wong KY. Health checks through landmark bridges to sky-high structures. *Proceedings of 5th International Workshop on Advanced Smart Materials and Smart Structures Technology*, Boston; 2009, p. 9–22.
14. Myung H, Lee SM. Lee BJ. *Paired structured light for structural health monitoring robot system Structural Health Monitoring* 2011; **10**(1):49–64.
15. Myung H, Jung JD, Jeon H. Robotic SHM and model-based positioning system for monitoring and construction automation. *Advances in Structural Engineering* 2012; **15**(6):943–954.
16. Jeon H, Bang Y, Myung H. A paired visual servoing system for 6-DOF displacement measurement of structures. *Smart Materials and Structures* 2011; **20**(4):45019.
17. Jeon H, Shin JU, Myung H. Incremental displacement estimation of structures using paired structured light. *Smart Structures and Systems* 2012; **9**(3):273–286.
18. Jeon H, Shin JU, Myung H. The displacement estimation error back-propagation (DEEP) method for a multiple structural displacement monitoring system. *Measurement Science and Technology* 2013; **24**(4):45104.
19. Jeon H, Myeong W, Shin JU, Park JW, Jung HJ, Myung H. Experimental validation of ViSP for structural displacement monitoring. *IEEE/ASME Transactions on Mechatronics* 2014; **19**(5):1603–1611.
20. Vaughan CL. Smoothing and differentiation of displacement-time data: an application of splines and digital filtering. *International Journal of Bio-Medical Computing* 1982; **13**(5):375–386.
21. Chen L, Arambel PO, Mehra RK. *Fusion Under Unknown Correlation - Covariance Intersection as a Special Case*. Washington: Proceedings of International Society of Information Fusion Conference, 2002; 905–912.
22. Myung H, Lee HK, Choi K, Bang S. Mobile robot localization with gyroscope and constrained kalman filter. *International Journal of Control, Automation and Systems* 2010; **8**(3):667–676.
23. Suh YS. Orientation estimation using a quaternion-basaed indirect kalman filter with adaptive estimation of external acceleration. *IEEE Transactions on Instrumentation and Measurement* 2010; **59**(12):3296–3305.
24. Xsens, Inc. The next generation Xsens motion trackers for industrial applications. 2014; Available: http://www.xsens.com
25. Optex-FA. Optex-FA sensor head instruction manual displacement sensor CD4 series. 2007; Available: http://www.optex-ramco.com
26. Thorlabs, Inc. Thorlabs' V21 photonics catalog. 2011; Available: http://www.thorlabs.com
27. Lee JH, Ho HN, Shinozukz M, Lee JJ. An advanced vision-based system for real-time displacement measurement of high-rise buildling. *Smart Materials and Structures* 2012; **21**(12):125019.
28. Chapra SC. *Applied Numerical Methods with MATLAB for Enginners and Scientists* (3rd edn). McGraw-Hill, 2012.

DOI: 10.1002/stc